Wind power distribution over the ocean

W. Timothy Liu,[1] Wenqing Tang,[1] and Xiaosu Xie[1]

Received 4 April 2008; revised 22 May 2008; accepted 3 June 2008; published 8 July 2008.

[1] Probability distribution and power density of wind speed over global oceans are computed from eight years of QuikSCAT measurements. They describe the variation and higher moments of wind speed that are critical in relating the non-linear effects of wind on electric power generation capability, shipping hazard, and air-sea exchanges in heat, water, and greenhouse gases. The power density distribution confirms our general knowledge of atmospheric circulation related to mid-latitude storm tracks, trade winds, and monsoons. It also reveals regions of high wind power associated with flow distortion by land, wind channeled by land topography, and buoyancy effect on turbulent stress driven by ocean fronts. **Citation:** Liu, W. T., W. Tang, and X. Xie (2008), Wind power distribution over the ocean, *Geophys. Res. Lett.*, *35*, L13808, doi:10.1029/2008GL034172.

1. Introduction

[2] With the increasing demand of electric power and the need of reducing greenhouse gas emission, the importance of turning wind energy at sea into electric power has never been more evident. New technology has enabled floating wind-farms in the open seas to capture the higher wind energy and reduce the environmental impact on the coastal regions. The white paper on energy [*Department of Trade and Industry*, 2007] lays out an ambitious plan to the British Parliament in meeting the Renewables Obligation with offshore wind energy. The Paper posted a challenge not only to Denmark, the leader of European offshore wind energy, but also to the world. Detailed distribution of wind power density (E), as defined in section 2, is needed to optimize the deployment of such wind farms.

[3] The distribution of strong winds over ocean is also needed to avoid hazard conditions for shipping. Operational numerical weather prediction (NWP) products have been shown to be deficient in describing the detailed structures and capturing the high wind events. Forecasters have used space-based ocean wind-stress measurements in making wind warning and forecast decision related to tropical and extra-tropical cyclones. By filling data gaps and detecting strong winds, the Ocean Prediction Center of the United States made dramatic increases in detecting extratropical storms with hurricane strength after using data from the scatterometer on QuikSCAT [*Von Ahn et al.*, 2006].

[4] Strong wind affects mixing in the ocean and the atmosphere and the ocean-atmosphere exchanges in momentum, heat, water, and gases. Such exchanges affect energy/water/carbon cycles and climate changes [e.g., *Liu et al.*, 1979; *Carr et al.*, 2002].

[5] *Liu et al.* [2008] discussed the impact on our understanding of the diurnal variation of E by using wind-stress from two identical scatterometers flying in tandem for six months. We will examine the variation of E from a few days to a few years, using eight years of QuikSCAT data. The computation of E is described in section 2. The conventional knowledge is confirmed in section 3, examples of regional features observed from space are given in section 4, and the temporal variations of the probability distribution function (PDF) are described in section 5.

2. Data and Processing

[6] The capability of the space-based scatterometer in measuring strong wind at high spatial resolution is discussed by *Liu* [2002] and *Liu and Xie* [2006]. The scatterometer sends microwave pulses to the Earth's surface and measures the backscatter power. Over the ocean, the backscatter power is largely caused by small centimeter-scale waves on the surface, which are believed to be in equilibrium with stress (τ). Stress is the turbulent momentum transfer generated by vertical wind shear and buoyancy. *Liu and Large* [1981] demonstrated, for the first time, the relation between measurements by a space-based scatterometer and surface stress measured on research ships. There were not sufficient direct stress measurements to calibrate the scatterometer. The geophysical data product of the scatterometer is the Equivalent Neutral Wind (ENW) at 10 m height [*Liu and Tang*, 1996], which, by definition, is uniquely related to τ, while the relation between τ and the actual winds at the reference level depends on atmosphere stability and ocean's surface current. Although the scatterometer has been known to measure τ, it has also been promoted as a wind-measuring instrument. ENW has been used as the actual wind, particularly in operational weather applications. The difference between the variability of stress and wind is assumed to be negligible because the marine atmosphere has near neutral stratification, and the magnitude of ocean current is small relative to wind speed over most ocean areas.

[7] Scattorometer climatology in forms of mean wind [e.g., *Risien and Chelton*, 2006] and the frequency of strong wind [*Sampe and Xie*, 2007] has been produced. We will analyze PDF and E, which will provide the characteristics of not only the means and the frequencies of high values of wind, but also the variation and higher moment critical in relating the non-linear effects of wind on electric power generation capability, shipping hazard, and air-sea exchanges.

[8] QuikSCAT Level-2 data at 12.5 km resolution are obtained from the Physical Oceanography Data Active Archive Center. Eight years of the data, from January

[1]Jet Propulsion Laboratory, California Institute of Technology, Pasadena, California, USA.

0094-8276/08/2008GL034172

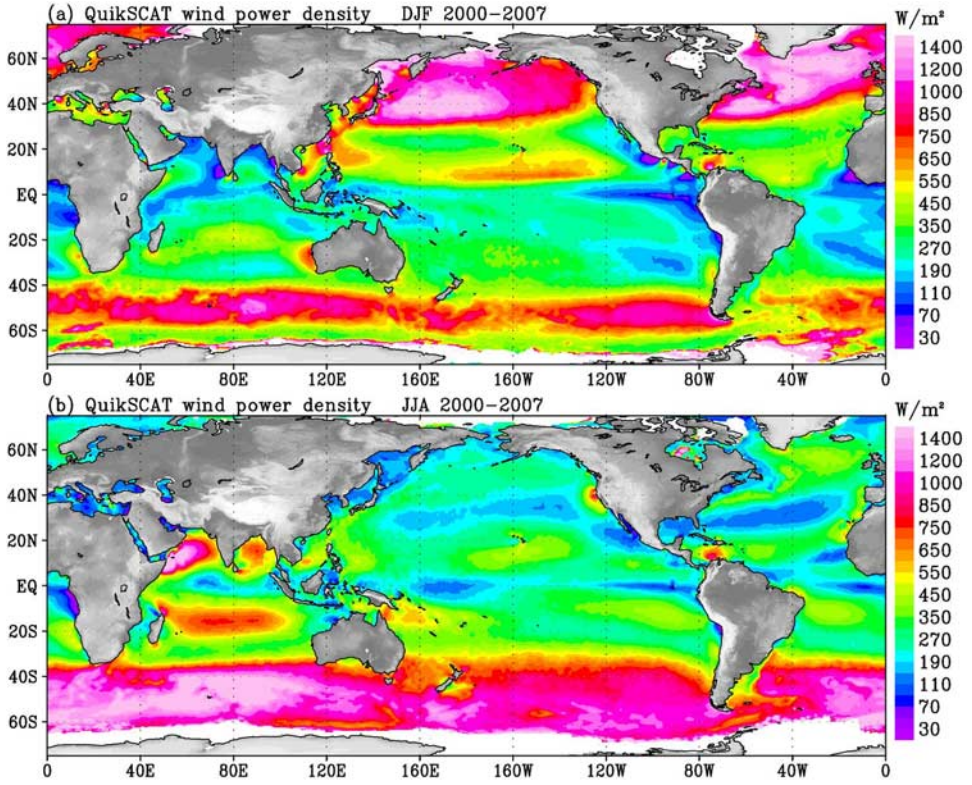

Figure 1. Distributions of wind power density derived from QuikSCAT for (a) boreal winter (December, January, and February) and (b) boreal summer (June, July, and August), for a eight year period between 2000 and 2007. The grey scale is used to show land topography.

2000 to December 2007, organized in wind vector cells along satellite swath, are binned into uniform 1/8 degree grids over global oceans fitted to the Weibull distribution for monthly, seasonal, and yearly periods. The Weibull distribution (Gaussian and Rayleigh distributions are special cases of it) has been often used to characterize the PDF of wind power [e.g., *Pavia and O'Brien*, 1986]. A two parameters Weibull distribution has the PDF (p) as a function of wind speed U,

$$p(U) = (k/c)(U/c)^{k-1} \exp\left[-(U/c)^{k}\right] \quad (1)$$

where k is the dimensionless shape parameter, and c is the scale parameter. A number of methods to estimate Weibull parameters exist, with negligible difference in the results [*Monahan*, 2006]. We used the simplest formula:

$$c = \overline{U}/\Gamma(1 + 1/k) \quad (2a)$$

$$k = \left(\overline{U}/\sigma\right)^{1.086} \quad (2b)$$

where $\overline{U}$ is the mean, σ is the standard deviation of wind speed, and Γ is the gamma function. The available wind power density E (which is proportional to U^3) may be calculated from the Weibull distribution parameters as

$$E = \tfrac{1}{2}\, \rho\, c^3\, \Gamma(1 + 3/k) \quad (3)$$

where ρ is the air density. E is essentially the kinetic energy of the wind. Gas exchange coefficient should have similar characteristics. There is hardly any in situ stress measurement. Even for winds, there is no in situ measurement that could represent the range of scatterometer data, particularly at the high and low ends, to evaluate the PDF of scatterometer data from which E is derived.

3. Large Scale Distribution

[9] The distribution of E, as shown in Figure 1, confirms the conventional knowledge – strongest E is found over the mid-latitude storm tracks of the winter hemisphere, the relatively steady trade winds over the tropical oceans, and the seasonal monsoons. At mid-latitude in the winter hemisphere, E is much larger than those in the tropics, making the display of the major features with the same color scale extremely difficult. The trade winds, particularly in the western Pacific and Southern Indian oceans are stronger in winter than summer, but the seasonal contrast is much less than those of the mid-latitude storm track. In the East China Sea, particularly through the Taiwan and Luzon Straight, the strong wind is caused by the winter monsoon. In the Arabian Sea and Bay of Bengal, the strong wind is

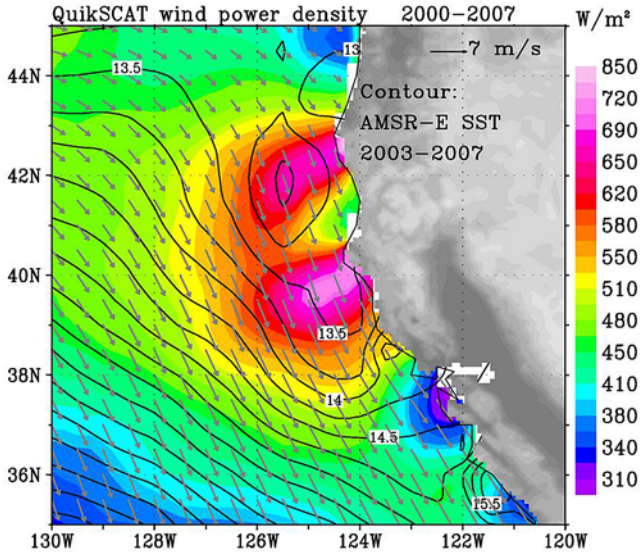

Figure 2. Same as Figure 1, but for annual mean and with superimposition of QuikSCAT equivalent neutral wind vectors (arrows) for the same period, and isotherm of SST derived from the Advanced Microwave Scanning Radiometer - EOS (AMSR-E) for a five year period (2003–2007), off the west coast of United States.

caused by the summer monsoon. In the South China Sea, the wind has two peaks, both in summer and winter. QuikSCAT data also reveal detailed wind structures not sufficiently identified before. The strong winds of transient tropical cyclones are not evident in E derived from the eight-year ensemble.

4. Regional Features

4.1. Aerodynamics

[10] Regions with high E associated with the acceleration of strong prevailing winds when deflected by protruding landmass are ubiquitous. When the westerlies over the southern oceans blow around Tasmania, South Island of New Zealand, and Tierra del Fuego, they create wind shadows as well as strong jets. Similarly strong jets are formed when the Southeast Trade is deflected at Cape d'Ambre and Cape Sainte Marie at the north and south tips of Madagascar. Asian monsoons are strengthened offshore from Phan Rang in Vietnam and at Dandra Head in Sri Lanka. Figures 2 and 3 show two examples of such strong jets in less well-known regions. Strong E is found downwind of Cape Blanco and Cape Mendocino in the United States (Figure 2), with northerly winds year round (strongest in summer) stirring up two centers of low ocean temperature. Similar features are found downwind Peninsula de La Guajira in Columbia (Figure 3), with easterly winds year round (weakest in fall).

4.2. Land Topography

[11] Strong E is also found (Figure 1) when strong wind blows offshore, channeled by topography. There were many studies on the wind jets through the mountain gap of Tehuantepec in Mexico [e.g., *Xie et al.*, 2005; *Sun and Yu*, 2006]. The well-known mistral blowing down to the Mediterranean from the gaps between Spain and France [e.g., *Guénard et al.*, 2006] is also obvious in Figure 1. Another example is shown in Figure 4, with strong wind blowing through mountain gap south of Vladivostok causing cooling in the Japan Sea [*Kawamura and Wu*, 1998]. These north/northwesterly winds then blow across the mountain of Japan and form strong wind jet west of Izu Islands [*Sampe and Xie*, 2007]. Transient wind jets, such as the Santa Ana winds through the mountain passes and canyons of Southern California [*Hu and Liu*, 2003], do not significantly affect the long-term distribution.

4.3. Ocean Front

[12] Alternate high and low E caused by the sea surface temperature (SST) modification of wind-stress at the semi-permanent meanders of the mid-latitude currents, such as the Agulhas Extension [*Liu et al.*, 2007], the Kuroshio Extension [*Liu and Xie*, 2008], and the Gulf Streams are

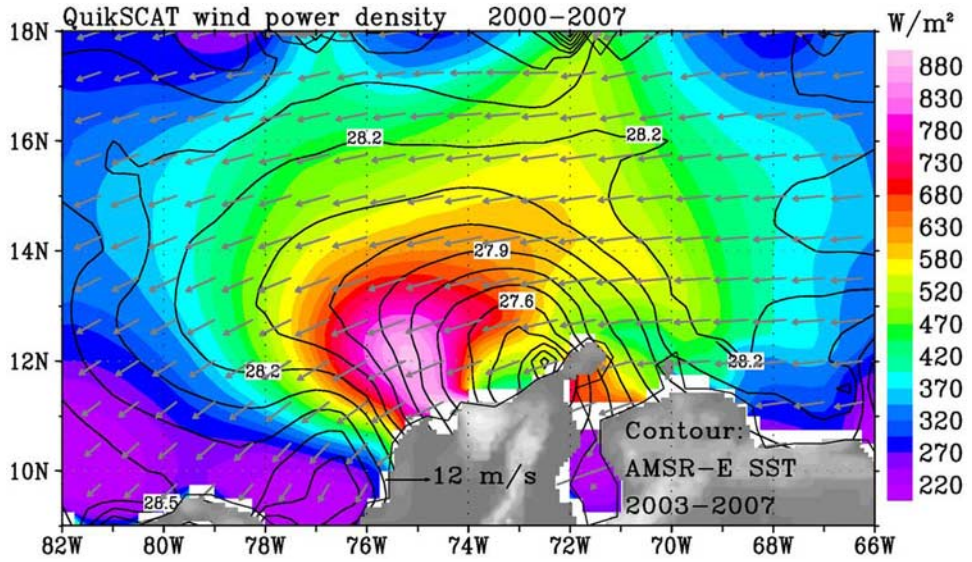

Figure 3. Same as Figure 2, except for a region in the Caribbean.

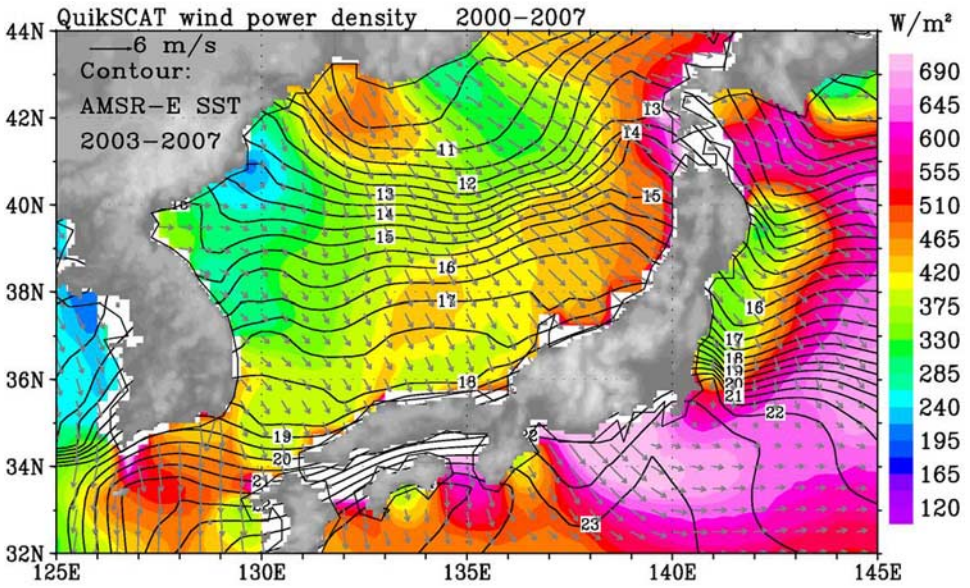

Figure 4. Same as Figure 2, except for a region in the western North Pacific.

clearly identified. Figure 5 shows the ocean-atmospheric interaction around the Gulf Stream and Labrador Sea. A semi-stationary cold eddy is clearly identified southeast of Newfoundland at 45°N and 51°W [e.g., *Rossby*, 1996], with a large drop of ENW and E. North of this cold eddy, the northwestward intrusion of warm water into the southern Labrador Sea is collocated with high E.

[13] As indicated by *Liu et al.* [2007] and *Liu and Xie* [2008], the reason for the good collocation of high and low ENW and SST, is that at the small scales turbulence (stress) generation by buoyancy, large-scale dynamic factors are not significant. How the strong horizontal ocean temperature gradient and current shear at mid-latitude ocean fronts are propagated up the atmosphere, through stress, and reflected in horizontal distribution of wind at various levels in the atmosphere remains to be vigorously examined.

[14] Figure 5 also shows that the along shore wind coming down from the Labrador sea along the Greenland coast accelerates as it passes over Cape Farewell meeting with the wind blowing south along the Greenland coast facing the Atlantic, forming a strong wind jet. This is an example of conditions discussed in section 4.1.

5. Probability Distribution Function

[15] Figure 6 confirms that the PDF of wind speed over high latitude ocean is boarder than that over the tropical and subtropical ocean. At high latitudes, the seasonal cycle is

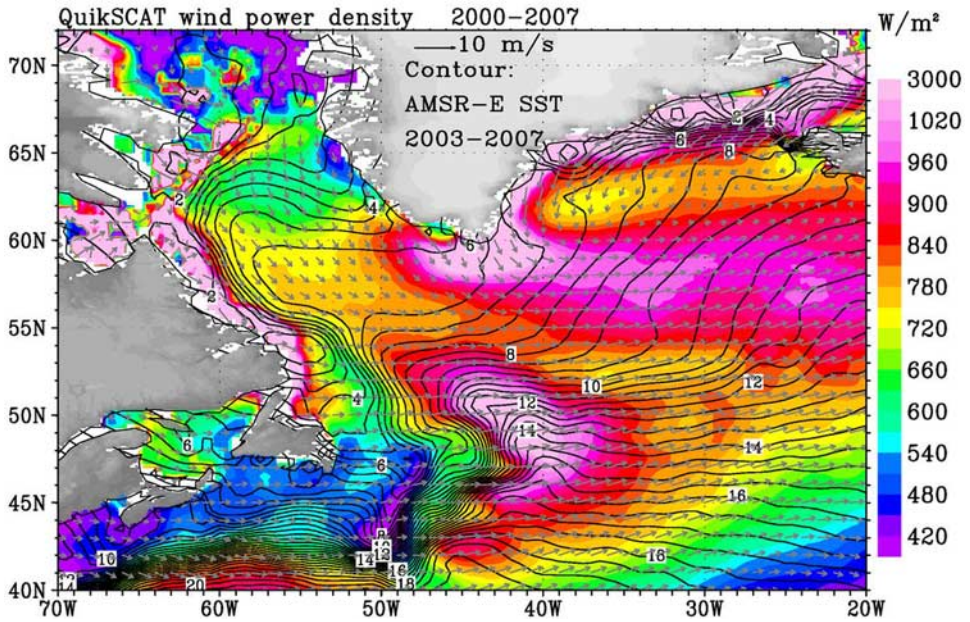

Figure 5. Same as Figure 2, except for the western North Atlantic.

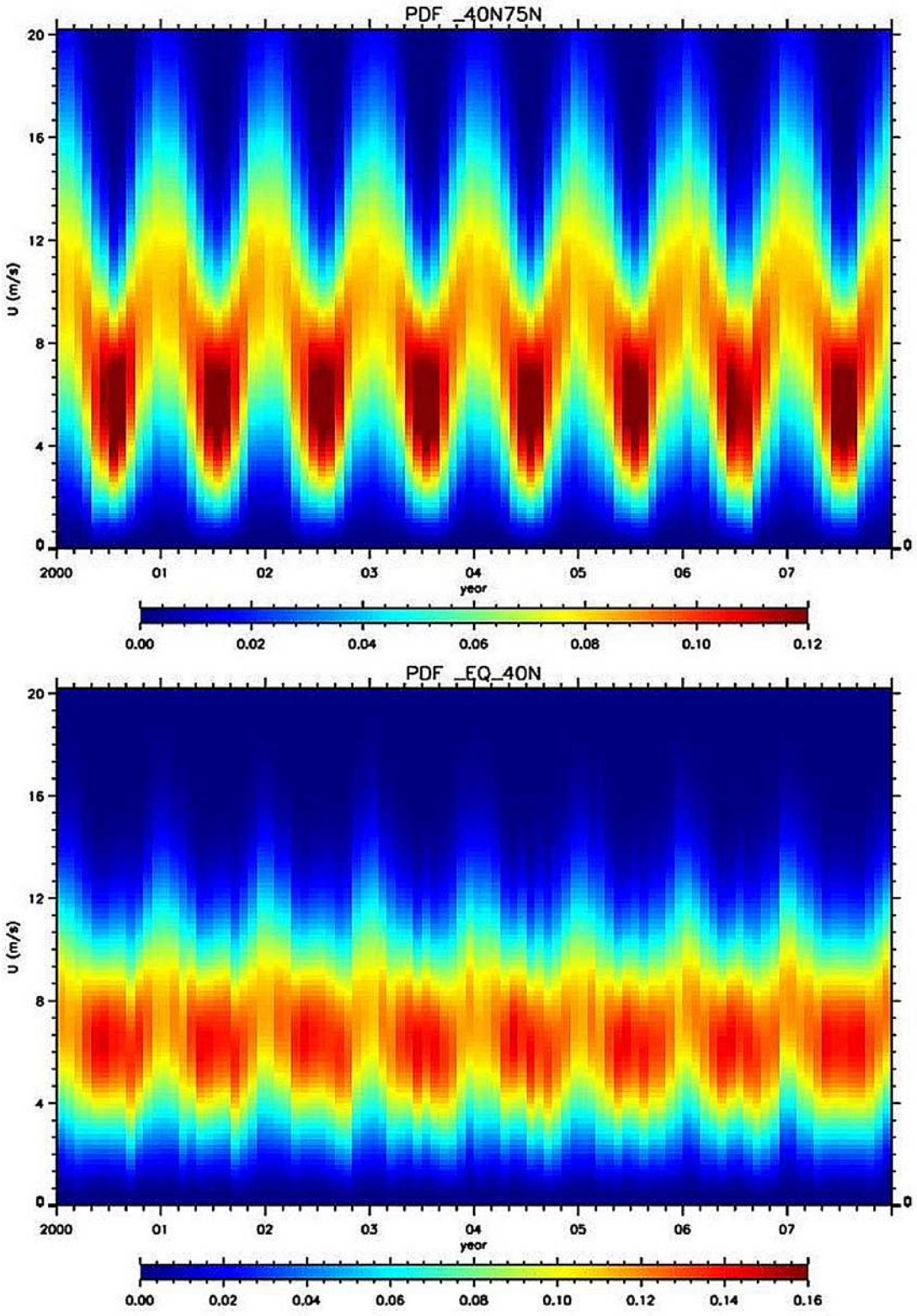

Figure 6. Temporal variation of the probability density function of QuikSCAT equivalent neutral wind speed averaged over all ocean area from (top) 40°N to 75°N, and (bottom) the Equator to 40°N.

much more pronounced with dominantly low speed during summer. The PDF in the Southern Hemisphere (not shown) is similar with less pronounced seasonal cycle as the Northern Hemisphere. Interannual and longer-term variations appear to be similar at all wind speed categories.

6. Discussion

[16] The distribution of E confirms the general knowledge of the large-scale atmospheric circulation including mid-latitude storm tracks, trade winds, and monsoons. The data reveal three causes of regional characteristics: land mass deflection of the surface flow, the gap wind channeled by land topography, and surface stress variation produced by atmospheric buoyancy driven by ocean front. The climatology (twelve calendar months) of PDF and E compiled from the eight years of QuikSCAT measurement is accessible at http://airsea.jpl.nasa.gov/; they should provide information of, not only the spatial variation, but also the temporal variation for wind regimes with various strength.

[17] **Acknowledgments.** This study was performed at the Jet Propulsion Laboratory, California Institute of Technology, under contract with the National Aeronautics and Space Administration (NASA). It was jointly supported by the Ocean Vector Wind and Physical Oceanography Program of NASA.

References

Carr, M., W. Tang, and W. T. Liu (2002), CO_2 exchange coefficients from remotely sensed wind speed measurements: SSM/I versus QuikSCAT in 2000, *Geophys. Res. Lett.*, *29*(15), 1740, doi:10.1029/2002GL015068.

Department of Trade and Industry (2007), Meeting the energy challenge: A white paper on energy, 341 pp., Stationary Off., London.

Guénard, V., P. Drobinski, J. L. Caccia, G. Tedeschi, and P. Currier (2006), Dynamics of the MAP IOP 15 severe mistral event: Observations and high-resolution numerical simulations, *Q. J. R. Meteorol. Soc.*, *132*, 757–777.

Hu, H., and W. T. Liu (2003), Oceanic thermal and biological responses to Santa Ana winds, *Geophys. Res. Lett.*, *30*(11), 1596, doi:10.1029/2003GL017208.

Kawamura, H., and P. Wu (1998), Formation mechanism of Japan Sea proper water in the flux center off Vladivostok, *J. Geophys. Res.*, *103*, 21,611–21,622.

Liu, W. T. (2002), Progress in scatterometer application, *J. Oceanogr.*, *58*, 121–136.

Liu, W. T., and W. G. Large (1981), Determination of surface stress by Seasat-SASS: A case study with JASIN data, *J. Phys. Oceanogr.*, *11*, 1603–1611.

Liu, W. T., and W. Tang (1996), Equivalent neutral wind, *JPL Publ.*, *96-17*, 16 pp.

Liu, W. T., and X. Xie (2006), Measuring ocean surface wind from space, in *Remote Sensing of the Marine Environment*, *Manual Remote Sens.*, vol. 6, 3rd ed., edited by J. Gower, chap. 5, pp. 149–178, Am. Soc. for Photogramm. and Remote Sens., Bethesda, Md.

Liu, W. T., and X. Xie (2008), Ocean-atmosphere momentum coupling in the Kuroshio Extension observed from space, *J. Oceanogr.*, in press.

Liu, W. T., K. B. Katsaros, and J. A. Businger (1979), Bulk parameterization of air-sea exchanges in heat and water vapor including the molecular constraints at the interface, *J. Atmos. Sci.*, *36*, 1722–1735.

Liu, W. T., X. Xie, and P. P. Niiler (2007), Ocean-atmosphere interaction over Agulhas Extension meanders, *J. Clim.*, *20*, 5784–5797.

Liu, W. T., W. Tang, X. Xie, R. Navalgund, and K. Xu (2008), Power density of ocean surface wind-stress from international scatterometer tandem missions, *Int. J. Remote Sens.*, in press.

Monahan, A. H. (2006), The probability distribution of sea surface wind speeds. Part I: Theory and SeaWinds observations, *J. Clim.*, *19*, 497–520.

Pavia, E. G., and J. J. O'Brien (1986), Weibull statistics of wind speed over the ocean, *J. Clim. Appl. Meteorol.*, *25*, 1324–1332.

Risien, C. M., and D. B. Chelton (2006), A satellite-derived climatology of global ocean winds, *Remote Sens. Environ.*, *105*, 221–236.

Rossby, T. (1996), The North Atlantic current and surrounding waters: At the crossroads, *Rev. Geophys.*, *34*, 463–481.

Sampe, T., and S.-P. Xie (2007), Mapping high sea winds from space: A global climatology, *Bull. Am. Meteorol. Soc.*, *88*, 1965–1978.

Sun, F., and J.-Y. Yu (2006), Impacts of Central America gap winds on the SST annual cycle in the eastern Pacific warm pool, *Geophys. Res. Lett.*, *33*, L06710, doi:10.1029/2005GL024700.

Von Ahn, J., J. M. Sienkiewicz, and P. Chang (2006), Operational impact of QuikSCAT winds at the NOAA Ocean Prediction Center, *Weather Forecasting*, *21*, 523–539.

Xie, S.-P., H. Xu, W. S. Kessler, and M. Nonaka (2005), Air-sea interaction over the eastern Pacific warm pool: Gap winds, thermocline dome, and atmospheric convection, *J. Clim.*, *18*, 5–20.

W. T. Liu, W. Tang, and X. Xie, Jet Propulsion Laboratory, California Institute of Technology, 4800 Oak Grove Drive, Pasadena, CA 91109-8099, USA. (w.timothy.liu@jpl.nasa.gov)